Kinetics and Mechanism of Ethane Oxidation to Acetic Acid on Catalysts Based on Mo−V−Nb Oxides

Xuebing Li and Enrique Iglesia*

Department of Chemical Engineering, University of California, Berkeley, California 94720-1462

Received: February 19, 2008; Revised Manuscript Received: May 5, 2008

Kinetic and isotopic studies showed that C−H bond activation in ethane by surfaces essentially saturated with lattice oxygens is the sole kinetically relevant step in ethane oxidation on Mo−V−NbO_x mixed oxides. These conclusions are consistent with the dependence of oxidation rates on O_2 and C_2H_6 pressures, with H/D exchange and kinetic isotope effects, and with the preferential initial incorporation of ^{16}O atoms from the oxide lattice into products formed from $^{18}O_2-C_2H_6$ mixtures. The precipitation of active components ($Mo_{0.61}V_{0.31}Nb_{0.08}O_x$) in the presence of colloidal TiO_2 led to 10-fold increases in all rate constants (per active component), consistent with higher dispersion of active components resembling in structure and surface reactivity those prevalent in bulk powders. The concurrent presence of PdO_x cocatalyst, even as a separate solid, markedly increased all rate constants for oxidation of ethene intermediates and specifically that for ethene oxidation to acetaldehyde molecules, which are rapidly converted to acetic acid on active Mo−V−NbO_x sites. Water, whether formed as a byproduct or added with $C_2H_6-O_2$ reactants, increases acetic acid selectivities by promoting the desorption of adsorbed acetate species as acetic acid. Ethene molecules, formed as reactive intermediates, inhibit ethane oxidation rates by depleting surface lattice oxygen atoms in fast oxidation reactions, thus decreasing the number of sites available at steady state for the kinetically relevant C−H bond activation step required for ethane conversion.

1. Introduction

Available alkane feedstocks and stable inorganic catalysts make direct oxidation of ethane[1] an attractive alternative to methanol carbonylation with homogeneous Rh and Ir complexes requiring halogen cocatalysts[2] for the synthesis of acetic acid. Mixed Mo−V−Nb oxides catalyze oxidation of ethane, ethene, or ethanol to acetic acid[1,3–6] and oxidation of propane and propene to acrylic acid.[7–11] Acetic acid synthesis rates and yields from ethane and ethene reactants increased when Mo−V−Nb oxides were combined with traces of Pd,[5,12,13] because PdO_x species catalyze ethene oxidation to acetaldehyde, which then reacts to form more stable acetic acid on active sites in mixed oxides.[4,5] We recently showed that rates of ethane, ethene, and ethanol oxidation to acetic acid increase when active Mo−V−Nb oxides were precipitated in the presence of colloidal TiO_2 to form materials with much higher active areas, but apparently with similar structure and surface properties as unsupported powders. These dispersion improvements and the presence of Pd-based cocatalysts led to unprecedented rates of acetic acid synthesis from ethane, ethene, and ethanol feedstocks.[3–5]

Here, we provide kinetic and isotopic evidence for the identity, reversibility, and kinetic relevance of elementary steps involved in ethane conversion to acetic acid and for the dynamics of primary and secondary oxidation steps. These data show that TiO_2 supports merely increase rate constants for all primary and secondary reactions, while Pd sites selectively increase ethene oxidation rates and shift the reaction selectivity from ethene to acetic acid. Ethane activation proceeds via kinetically relevant C−H bond activation on surface lattice oxygen atoms, consistent with normal H/D kinetic isotope effects, while oxygen vacancies involved as intermediates are replenished rapidly via rapid diffusion of bulk lattice oxygen atoms and irreversible O_2 dissociation steps.

2. Experimental Section

2.1. Catalyst Synthesis. A slurry method was used to synthesize Mo−V−Nb oxides in the presence or absence of colloidal TiO_2.[1,5] A solution of ammonium niobate(V) oxalate hydrate ($C_4O_8NbOH\cdot NH_3$; Aldrich; 99.99%) was added slowly to another solution containing oxalic acid ($C_2O_4H_2$; Fluka, 99%), ammonium (meta)vanadate (NH_4VO_3; Sigma-Aldrich, 99%), and ammonium heptamolybdate ($(NH_4)_6Mo_7O_{24}*4H_2O$; Aldrich, 99.98%) while being stirred at ambient temperature. The atomic Mo:V:Nb ratio was 0.61:0.31:0.08. The powders formed (12 g) were treated at 393 K overnight in ambient air and then in flowing dry air (Praxair, extra dry, 1.67 $cm^3\ s^{-1}$) at 673 K for 4 h. TiO_2 (P25 from Degussa, BET: 50 m^2/g, anatase/rutile = 3) was added to the $C_2O_4H_2$, NH_4VO_3, and $(NH_4)_6Mo_7O_{24}*4H_2O$ solution before being mixed with the $C_4O_8NbOH\cdot NH_3$ solution to synthesize the 24 wt % $Mo_{0.61}V_{0.31}Nb_{0.08}O_x/TiO_2$ sample. A Pd/SiO_2 sample (0.3 wt % Pd) was physically mixed with $Mo_{0.61}V_{0.31}Nb_{0.08}O_x/TiO_2$ to prepare a sample with 0.0025 wt % Pd. Pd/SiO_2 was prepared by suspending silica (Cab-O-Sil, 99.8%) in a solution of tetraamminepalladium(II) nitrate (6.7×10^{-3} M; $[Pd(NH_3)_4](NO_3)_2$; Aldrich, 99.99%). The suspended solids (10 g) were dried at 393 K overnight in static air and then treated in flowing dry air (Praxair, extra dry, 1.67 $cm^3\ s^{-1}$) at 773 K for 4 h.

2.2. Ethane Oxidation Rates and Selectivities. Ethane oxidation rates and selectivities were measured in a packed-bed flow reactor using catalyst aggregates (0.25−0.50-mm diameter; 0.2 g) diluted with quartz (2.8 g; Aldrich, acid-washed) to prevent temperature gradients. All transfer lines were kept above 433 K to avoid condensation. C_2H_6 (Praxair, 99.999%), He (Praxair, 99.999%), and N_2/O_2 (Praxair mixture, 10% N_2 in

* Corresponding author. E-mail: iglesia@berkeley.edu.

10.1021/jp801488y CCC: $40.75
Published on Web 08/29/2008

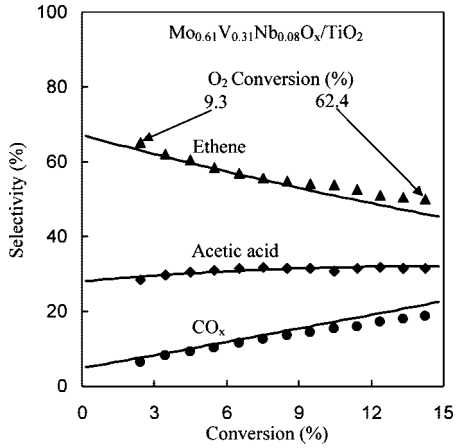

Figure 1. Product selectivities of ethane oxidation at 573 K on $Mo_{0.61}V_{0.31}Nb_{0.08}O_x/TiO_2$ versus ethane conversion. Solid lines (—) are predicted selectivities from eqs 1–3. C_2H_6: 533 kPa; O_2: 107 kPa; H_2O: 320 kPa.

O_2, certified) flow rates were controlled by mass flow controllers (Porter). H_2O (deionized, resistivity > 18.0 MΩ cm) was introduced with a high-pressure syringe pump (Teledyne Isco Inc., model 500 D). Catalysts were treated in flowing mixtures of He (Praxair, 99.999%, 0.49 $cm^3\ s^{-1}$) with N_2/O_2 (Praxair mixture, 10% N_2 in O_2, certified, 0.09 $cm^3\ s^{-1}$) flow at 673 K for 2 h. Effluent streams were analyzed by gas chromatography (HP 5890, II). N_2, O_2, CO, CO_2, and H_2O were separated in an HP Plot Q capillary column (30 m × 0.32 mm) and detected by thermal conductivity. C_2H_6, C_2H_4, and CH_3COOH were separated in an HP Plot U capillary column (30 m × 0.32 mm) and detected by flame ionization.

Isotopic experiments were carried out in a gradientless recirculating batch reactor (206 cm^3 volume). All internal reactor surfaces were coated with SiO_2 (Entech Instruments) to prevent side reactions and kept at ~433 K to avoid condensation. Reacting mixtures were circulated at 20 cm^3 (STP) s^{-1} using a graphite gear micropump (Micropump 182−336). C_2H_6 and O_2 conversions were kept below 1% per pass to ensure gradientless conditions and strict kinetic control. Chemical and isotopic compositions were measured by sampling the reactor contents into a gas chromatograph (HP 6890) equipped with a mass selective detector (HP 5973). Chemical species were separated with an HP Plot Q capillary column (30 m × 0.32 mm), and isotopomer concentrations were measured from mass spectra using deconvolution methods that account for natural isotopic abundance and fragmentation patterns;[14] these procedures allowed measurements of the content and position of ^{13}C, D, and ^{18}O within each molecular species. C_2D_6 (Isotec, isotopic purity >99%), $^{13}C_2H_4$ (Isotec, isotopic purity >99%), $^{18}O_2$ (Isotec, isotopic purity >99%), and $^{13}CH_3{}^{13}COOH$ (Isotec, isotopic purity >99%) were used in the highest purity available without further purification.

3. Results and Discussion

3.1. Reaction Network and Kinetics Analysis. Figure 1 shows selectivities to ethene, acetic acid, and CO_x on $Mo_{0.61}V_{0.31}Nb_{0.08}O_x/TiO_2$ at 573 K as a function of ethane conversion, which was varied by changing reactant residence time. Selectivities for ethene (68%), acetic acid (28%), and CO_x ($CO+CO_2$; 6%) extrapolated to zero conversion reflect their relative rates of formation during a single reactive sojourn of ethane reactants on active surfaces, without contributions from secondary reactions of primary ethene products. Their nonzero values indicate

SCHEME 1: Primary and Secondary Pathways for Ethane Oxidation on Catalysts Based on Mo−V−Nb Oxides

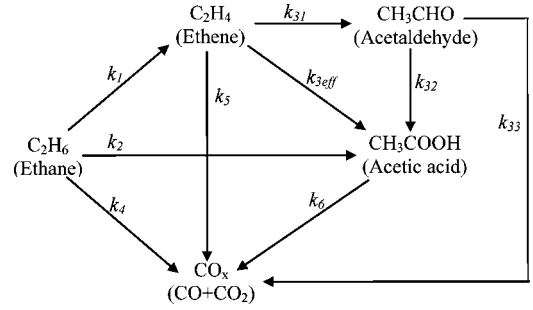

that all three products can form directly from ethane on Mo−V−Nb oxides, as previously found.[15,16] Specifically, acetic acid can form without intervening desorption of ethene and its subsequent oxidation, apparently via sequential α-hydrogen elimination steps from adsorbed ethoxides,[15,17] also involved as intermediates in dehydrogenation events. Measurements on unsupported $Mo_{0.61}V_{0.31}Nb_{0.08}O_x$ powders led to identical conclusions.

Rates of formation of each product extrapolated to zero residence time were used to measure first-order rate constants for primary steps that lead to ethene, acetic acid, and CO_x (k_1, k_2, and k_4 in Scheme 1, data in Table 1). The first-order dependence on ethane and the zero-order dependence on O_2 were determined by rate measurements as a function of ethane and O_2 pressures. Ethane oxidation rates (extrapolated to zero contact time) increased linearly with ethane pressure (0.53−1.07 MPa, Table 2), but primary selectivities were unaffected, indicating that all primary reactions are first-order in ethane reactants, as also reported on VO_x and MoO_x catalysts for oxidative dehydrogenation of alkanes.[18–20] Primary ethane oxidation rates and selectivities were not influenced by O_2 pressure (53−107 kPa, Table 2), suggesting that all reactions occur on surfaces saturated with active lattice oxygen atoms. These data are consistent with fast (and irreversible) reoxidation of vacancies formed as intermediates via sequential C−H bond activation and water desorption steps. The elementary steps involved in ethane oxidation to ethene and acetic acid are discussed in section 3.2, where measured kinetics are shown to be consistent with the proposed catalytic sequence when O* is the most abundant reactive intermediate. These kinetic features are typical of Mars van Krevelen cycles in which C−H bond activation is the kinetically relevant step.[18–20] The rate of ethene oxidation, which occurs as a secondary reaction during ethane oxidation, is also first-order in ethene and independent of O_2 pressure.[4]

Ethene oxidation on Mo−V−Nb oxides forms acetic acid as the predominant product and trace amounts of acetaldehyde as reactive intermediates.[4] PdO_x cocatalysts increase the rate of ethene oxidation to acetaldehyde, and the latter is then rapidly scavenged to form acetic acid via its subsequent oxidation on active Mo−V−Nb oxides.[4] As a result, acetic acid to ethene product ratios were much higher with PdO_x cocatalysts, which did not influence, however, ethane oxidation rates.[5]

Confirming evidence for primary acetic acid and CO_x synthesis pathways and independent values for the rate constants involved in secondary ethene reactions were obtained from the rates of formation of acetic acid and CO_x isotopomers formed in competitive oxidation of $^{13}C_2H_4$ (32 kPa)/$^{12}C_2H_6$ (533 kPa) reactant mixtures. Initial ^{12}C fractions in acetic acid (~0.4 on

TABLE 1: Rate Constants of Ethane Oxidation to Ethene and Acetic Acid[a]

sample	P_{H_2O} (kPa)	k_1[b]	k_2	k_{3eff}	k_4	k_5	k_6	$(k_1 + k_2)/k_4$	k_{3eff}/k_1	k_5/k_1
$Mo_{0.61}V_{0.31}Nb_{0.08}O_x$	320	0.098	0.030	0.38	0.006	0.17	0.30	21	3.9	1.7
$Mo_{0.61}V_{0.31}Nb_{0.08}O_x/TiO_2$	320	0.96	0.40	4.9	0.07	2.5	5.7	19	5.1	2.6
$Mo_{0.61}V_{0.31}Nb_{0.08}O_x/TiO_2$	0	1.44	0.26		0.15			11		
0.0025% Pd $Mo_{0.61}V_{0.31}Nb_{0.08}O_x/TiO_2$	320	0.76	0.39	102	0.09	14	4.0	13	134	18

[a] Reaction conditions: 573 K; partial pressures: ethane: 533 kPa; O_2: 107 kPa. [b] The unit of rate constant k_i is 10^{-5} mol g-atom-V^{-1} s^{-1} kPa^{-1}.

TABLE 2: Catalytic Oxidation of Ethane to Ethene and Acetic Acid at 573 K on $Mo_{0.61}V_{0.31}Nb_{0.08}O_x/TiO_2$ at Different Reactant Partial Pressures (H_2O Pressure: 320 kPa)

partial pressure (kPa)		primary selectivity[a] (%)			primary ethane oxidation rate[a] (10^{-3} mol-ethane g-atom V^{-1} s^{-1})
ethane	oxygen	ethene	acetic acid	CO_x	
1066	107	64	33	3	13.3
533	107	65	31	4	7.3
533	53	66	31	3	7.0

[a] The primary selectivities and ethane oxidation rates were obtained by extrapolating to zero contact time.

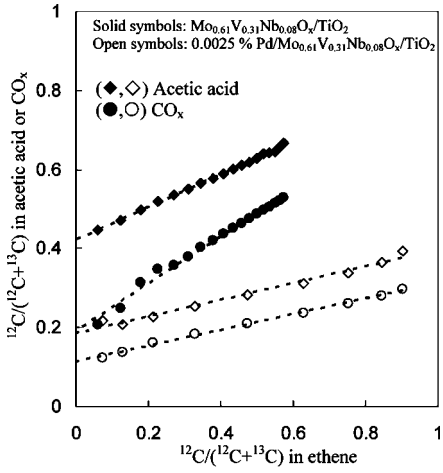

Figure 2. Fraction of ^{12}C in acetic acid and CO_x versus fraction of ^{12}C in ethene during $^{12}C_2H_6/^{13}C_2H_4/O_2$ mixture reaction on $Mo_{0.61}V_{0.31}Nb_{0.08}O_x/TiO_2$ and 0.0025% Pd $Mo_{0.61}V_{0.31}Nb_{0.08}O_x/TiO_2$ at 573 K. $^{12}C_2H_6$: 533 kPa; $^{13}C_2H_4$: 32 kPa; O_2: 107 kPa; H_2O: 320 kPa.

$Mo_{0.61}V_{0.31}Nb_{0.08}O_x/TiO_2$; ~0.2 on 0.0025% $Pd/Mo_{0.61}V_{0.31}Nb_{0.08}O_x/TiO_2$, Figure 2) and CO_x (~0.2 on $Mo_{0.61}V_{0.31}Nb_{0.08}O_x/TiO_2$; ~0.1 on 0.0025% $Pd/Mo_{0.61}V_{0.31}Nb_{0.08}O_x/TiO_2$, Figure 2) were nonzero, as expected from their formation, in part, via direct oxidation of ethane without the involvement of gas-phase ethene intermediates. PdO_x cocatalysts increased the rate of ethene-mediated secondary pathways, as well as their contribution to the total rate of acetic acid synthesis, consistent with the ability of Pd-based catalysts to catalyze intervening ethene to acetaldehyde steps. As a result, the initial ^{13}C fraction in acetic acid products was higher when PdO_x was present as a physical mixture with $Mo_{0.61}V_{0.31}Nb_{0.08}O_x$ catalysts.

Scheme 1 shows ethane oxidation pathways, including direct routes from ethane to ethene, acetic acid, and CO_x (CO and CO_2) and sequential ethene-mediated routes. The low acetaldehyde selectivities (<1%) observed at all conversions lead to pseudo-steady-state concentrations of acetaldehyde intermediates and to an effective rate constant k_{3eff} (in terms of true k_{31}, k_{32}, and k_{33}) for ethene oxidation to acetic acid via such reactive intermediates (derivation details in the Appendix). Also, contributions to CO_x via acetaldehyde intermediates are implicitly included in k_5 as a result of the assumption of pseudo-steady-state for reactive acetaldehyde intermediates.

CO_x forms also via sequential oxidation of primary ethene and acetic acid. Rate constants for secondary pathways, such as ethene oxidation to acetic acid and CO_x, cannot be accurately determined from the effects of residence time on selectivity, because of the complex connectivity within Scheme 1 and the potentially unequal inhibition of some of these steps by products, as discussed later. These first-order rate constants (k_{3eff}, k_5, and k_6 in Scheme 1) can be rigorously determined, however, by extrapolating the rates of formation of each ^{13}C-containing product to zero conversion in experiments using $^{13}C_2H_4$ (32 kPa)/$^{12}C_2H_6$ (533 kPa) and $^{13}CH_3{}^{13}COOH$ (32 kPa)/$^{12}C_2H_6$ (533 kPa) reactant mixtures (Table 1).[4]

Rate constants for each step in Scheme 1 are shown in Table 1 for $Mo_{0.61}V_{0.31}Nb_{0.08}O_x$, $Mo_{0.61}V_{0.31}Nb_{0.08}O_x/TiO_2$, and 0.0025 wt % $Pd/Mo_{0.61}V_{0.31}Nb_{0.08}O_x/TiO_2$ catalysts. The precipitation of active oxides in the presence of TiO_2 increased all rate constants about 10-fold, without significant effects on their relative values. These data indicate that such synthetic protocols merely increase active surface areas without concurrent effects on their intrinsic reactivity for primary and secondary steps. These conclusions are consistent with the similar areal ethane oxidation rates and product selectivities measured on bulk powders and on TiO_2-containing samples.[5]

In contrast, trace amounts of PdO_x selectively markedly increased rate constants for ethene oxidation to acetic acid (k_{3eff}) and CO_x (k_5), while ethane and acetic acid oxidation rate constants (k_1, k_2, k_4, and k_6) remained essentially unchanged. Neither TiO_2 nor PdO_x influenced the catalysis of primary ethane reactions, as shown by the similar $[(k_1 + k_2)/k_4]$ ratios measured on all catalysts. The presence of PdO_x markedly increased k_{3eff}/k_1 and k_5/k_1 ratios. It also led to k_{3eff}/k_1 ratios much larger than k_5/k_1 ratios, indicating that PdO_x cocatalysts selectively increased the rate of ethene oxidation to acetic acid synthesis without a commensurate increase in ethene combustion rates.

The expected effects of residence time (τ) on ethene, acetic acid, and CO_x selectivities (S_j), with the assumption that any inhibition by products equally affects all steps, are given by (derivation in Appendix):

$$S_{C_2H_4} = \frac{P_{C_2H_4}}{P^0_{C_2H_6} - P_{C_2H_6}} = \frac{\dfrac{k_1}{(k_{3eff} + k_5) - (k_1 + k_2 + k_4)} \cdot \left(e^{-(k_1+k_2+k_4)\cdot P^0_{C_2H_6}\cdot\tau} - e^{-(k_{3eff}+k_5)\cdot P^0_{C_2H_6}\cdot\tau}\right)}{1 - e^{-(k_1+k_2+k_4)\cdot P^0_{C_2H_6}\cdot\tau}} \quad (1)$$

$$S_{CH_3COOH} = \frac{P_{CH_3COOH}}{P^0_{C_2H_6} - P_{C_2H_6}} = \left[\frac{(k_2 \cdot ((k_{3eff} + k_5) - (k_1 + k_2 + k_4)) + k_1 \cdot k_{3eff})}{[(k_{3eff} + k_5) - (k_1 + k_2 + k_4)] \cdot (k_1 + k_2 + k_4 - k_6)} \cdot (e^{-k_6 \cdot P^0_{C_2H_6} \cdot \tau} - e^{-(k_1+k_2+k_4) \cdot P^0_{C_2H_6} \cdot \tau}) - \frac{k_1 \cdot k_{3eff}}{[(k_{3eff} + k_5) - (k_1 + k_2 + k_4)] \cdot (k_{3eff} + k_5 - k_6)} \cdot (e^{-k_6 \cdot P^0_{C_2H_6} \cdot \tau} - e^{-(k_3+k_5) \cdot P^0_{C_2H_6} \cdot \tau})\right] \Big/ [1 - e^{-(k_1+k_2+k_4) \cdot P^0_{C_2H_6} \cdot \tau}] \quad (2)$$

$$S_{CO_x} = 1 - S_{C_2H_4} - S_{CH_3COOH} \quad (3)$$

$$k_{3eff} = \frac{k_{31}}{1 + \frac{k_{33}}{k_{32}}} \cong k_{31} \quad (4)$$

where P_j is the pressure of species j and $P^0_{C_2H_6}$ is the ethane inlet pressure.

The effects of conversion on ethene, acetic acid, and CO_x selectivities predicted from eqs 1–3 are shown as solid lines in Figure 1 for $Mo_{0.61}V_{0.31}Nb_{0.08}O_x/TiO_2$. The excellent agreement with data confirms that any inhibition by products equally influences all primary and secondary steps and that similar active sites are involved in all steps. Any inhibition effects would then reflect competitive adsorption of products and reactants, probably via readsorption steps that merely reverse their desorption from such active sites.

3.2. Elementary Steps in Catalytic Ethane Oxidation Reactions. Next, we examine the elementary steps involved in primary reactions of ethane and their reversibility and kinetic relevance within the overall catalytic sequence using isotopic exchange and kinetic effects. Scheme 2 shows a sequence of reduction−oxidation elementary steps for ethane conversion to ethene and acetic acid, in which O* represents a surface lattice oxygen (M_i═O or M_i—O—M_j, where M_i and M_j can be Mo^{6+}, V^{5+}, or Nb^{5+}), CH_3CH_2O* is an ethoxide species attached to an M_i cation (C_2H_5—O—M_i), and CH_3CHO* and CH_3CO_2* are adsorbed acetaldehyde and acetate species, respectively. *OH denotes a hydroxyl group, and * represents an oxygen vacancy and its associated reduced center. Step 1 involves weak and quasi-equilibrated adsorption of ethane, from which hydrogen is subsequently abstracted by lattice oxygen atoms (step 2) to form chemisorbed ethoxides and *OH groups. Ethoxide species can undergo either β-hydride elimination to form ethene and *OH (step 3), or further oxidation via α-hydride abstraction by O* with acetic acid as the final product (steps 4, 6, 7, 8). Recombination of *OH groups forms H_2O and an oxygen vacancy (step 9) and oxygens are ultimately restored via irreversible dissociation of O_2 to complete a catalytic turnover (step 10).

SCHEME 2: Mars van Krevelen Redox Cycle for Ethane Oxidation to Ethene and Acetic Acid on Mo−V−Nb Oxide Catalysts

$C_2H_6 + O^*$	$\overset{K_1'}{\rightleftharpoons}$	$C_2H_6O^*$	[1]
$C_2H_6O^* + O^*$	$\xrightarrow{k_2'}$	$CH_3CH_2O^* + {}^*OH$	[2]
$CH_3CH_2O^*$	$\overset{K_3'}{\rightleftharpoons}$	$C_2H_4 + {}^*OH$	[3]
$CH_3CH_2O^* + O^*$	$\xrightarrow{k_4'}$	$CH_3CHO^* + {}^*OH$	[4]
CH_3CHO^*	$\overset{K_5'}{\rightleftharpoons}$	$CH_3CHO + *$	[5]
$CH_3CHO^* + {}^*O$	$\xrightarrow{k_6'}$	$CH_3CO^* + {}^*OH$	[6]
$CH_3CO^* + O^*$	$\xrightarrow{k_7'}$	$CH_3CO_2^* + *$	[7]
$CH_3CO_2^* + {}^*OH$	$\overset{K_8'}{\rightleftharpoons}$	$CH_3COOH + O^* + *$	[8]
$^*OH + {}^*OH$	$\overset{K_9'}{\rightleftharpoons}$	$H_2O + O^* + *$	[9]
$O_2 + * + *$	$\xrightarrow{k_{10}'}$	$O^* + O^*$	[10]

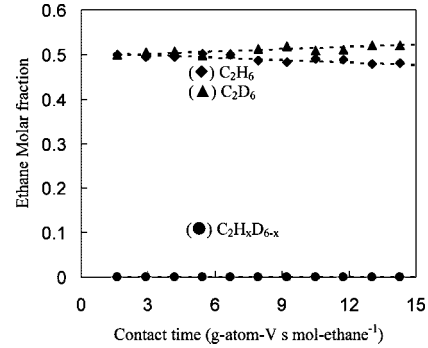

Figure 3. Deuterium distribution in ethane as a function of contact time during $C_2H_6/C_2D_6/O_2/H_2O$ mixture reaction on $Mo_{0.61}V_{0.31}Nb_{0.08}O_x/TiO_2$ at 573 K. C_2H_6: 266 kPa; C_2D_6: 266 kPa; O_2: 107 kPa; H_2O: 320 kPa.

These elementary steps, together with pseudo-steady-state assumptions for the most abundant adsorbed intermediates (O*, *OH, *, and C_2H_6O*) and quasi-equilibrium assumptions for steps 1 and 9, lead to the rate equation:

$$\text{rate} = \frac{k_2' \cdot K_1' \cdot P_{C_2H_6}}{\left[1 + \left(\frac{k_2' \cdot K_1' \cdot P_{C_2H_6}}{k_{10}' \cdot P_{O_2}}\right)^{1/2} + \left(\frac{k_2' \cdot K_1' \cdot P_{C_2H_6} \cdot P_{H_2O}^2}{k_{10}' \cdot K_9'^2 \cdot P_{O_2}}\right)^{1/4} + K_1' \cdot P_{C_2H_6}\right]^2} \quad (5)$$

The observed kinetic dependence of primary ethane oxidation rates on C_2H_6 and O_2 pressures (first-order in C_2H_6 and zero-order in O_2) is consistent with eq 5 when O* is the most abundant reactive intermediate:

$$\text{rate} = k_2' \cdot K_1' \cdot P_{C_2H_6} = (k_1 + k_2) \cdot P_{C_2H_6} \quad (6)$$

The apparent rate constants ($k_1 + k_2$) of primary pathways in Scheme 1 for ethene and acetic acid formation from ethane, are, therefore, given by $k_2' \cdot K_1'$. The reversibility, kinetic relevance, and consequences for kinetic inhibition by products can be inferred from the elementary steps in Scheme 2, as discussed in detail in the context of the isotopic studies described next.

3.2.1. Evidence for Irreversible C−H Bond Activation as the Sole Kinetically Relevant Step. The reversibility of C−H bond activation steps was probed by measuring the rate of isotopic exchange among ethane reactants during oxidation of $C_2H_6/C_2D_6/H_2O$ mixtures. Figure 3 shows that cross-exchange products ($C_2H_xD_{6-x}$; $0 < x < 6$) did not form at detectable rates. These data indicate that the reverse of C−H activation steps, which would lead to $C_2H_xD_{6-x}$ isotopomers, is at least 2 orders of magnitude slower than the rate of chemical conversion of ethane, where this limit reflects the detection threshold for $C_2H_xD_{6-x}$ isotopomers by mass spectrometry. The enrichment of the reacting mixture in C_2D_6 with time reflects its lower reactivity compared with that of C_2H_6, consistent with normal kinetic isotope effects that favor weaker C−H bonds over

TABLE 3: Kinetic Isotopic Effect of Ethane Oxidation to Ethene and Acetic Acid at 573 K on $Mo_{0.61}V_{0.31}Nb_{0.08}O_x/TiO_2$ (C_2H_6: 533 kPa; H_2O: 320 kPa or C_2D_6: 533 kPa; D_2O: 320 kPa)

	rate constants (10^{-5} mol g-atom-V^{-1} s^{-1} kPa^{-1})		
reactant	k_1	k_2	k_4
C_2H_6	0.97	0.40	0.07
C_2D_6	0.26	0.13	0.06
KIE (k_{i-H}/k_{i-D})	3.7	3.1	1.2

stronger C−D when their cleavage is required in kinetically relevant steps.

The kinetic relevance of C−H bond activation was confirmed by comparing rates for $C_2H_6/H_2O/O_2$ and $C_2D_6/D_2O/O_2$ reactants on $Mo_{0.61}V_{0.31}Nb_{0.08}O_x/TiO_2$ at 573 K. Rate constants for primary reactions (k_1, k_2, and k_4) with C_2H_6 and C_2D_6 reactants were measured by extrapolating ethene, acetic acid, and CO_x synthesis rates to zero contact time (Table 3). Normal kinetic isotopic effects (KIE) were observed for ethene (k_{1-H}/k_{1-D} = 3.7) and acetic acid (k_{2-H}/k_{2-D} = 3.1) synthesis; their similar values suggest a common kinetically relevant step, possibly the cleavage of C−H bonds in ethane to form ethoxide intermediates. The kinetic isotope effect for the combined rates of formation of ethene and acetic acid, which reflects this common C−H bond activation step, was 3.4. The KIE value for primary CO_x formation was much smaller (k_{4-H}/k_{4-D} = 1.2), suggesting that its formation did not require C−H bond cleavage in kinetically relevant steps and may occur on alternate active sites.[21] The transition states and intermediates involved in selective and unselective oxidation pathways appear to differ, as proposed on the basis of similar data for the case of oxidative alkane dehydrogenation on VO_x-based catalysts.[21]

3.2.2. Irreversible Oxygen Activation and Role of Bulk Lattice Oxygen. The reversibility of O_2 dissociation was probed by reactions of $^{18}O_2/^{16}O_2/C_2H_6/H_2{}^{16}O$ mixtures on $Mo_{0.61}V_{0.31}Nb_{0.08}{}^{16}O_x/Ti^{16}O_2$. Mixed $^{18}O^{16}O$ isotopomers were not detected (<1%) at any contact time or ethane conversion (Figure 4). Thus, O_2 formation via recombinative desorption of lattice oxygen atoms is >100 times slower than C−H bond activation steps and essentially irreversible during ethane oxidation. These data and conclusions are consistent with measured kinetic orders for ethane and O_2 reactants, which reflect rapid and irreversible reoxidation of vacancies involved in redox cycles, and with previous conclusion for oxidative alkane dehydrogenation on MoO_x, VO_x, and WO_x catalysts.[18–20]

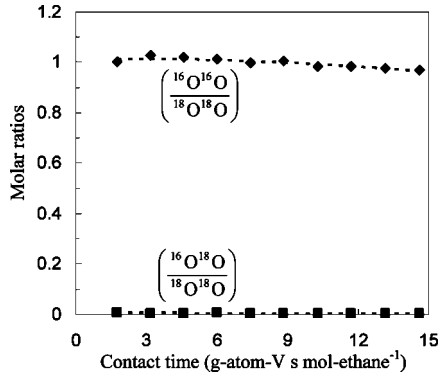

Figure 4. Oxygen isotopomer distributions as a function of contact time during reaction of $C_2H_6/^{16}O_2/^{18}O_2/H_2{}^{16}O$ mixture at 573 K on $Mo_{0.61}V_{0.31}Nb_{0.08}{}^{16}O_x/Ti^{16}O_2$. C_2H_6: 533 kPa; $^{16}O_2$: 53 kPa; $^{18}O_2$: 53 kPa; $H_2{}^{16}O$: 320 kPa.

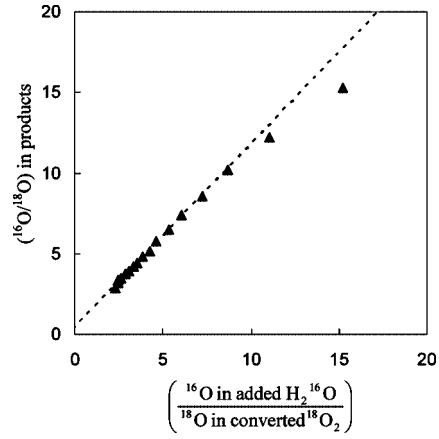

Figure 5. ($^{16}O/^{18}O$) ratio in the products (CH_3COOH, CO_2, CO, and H_2O) versus ratio of (^{16}O in added $H_2{}^{16}O/^{18}O$ in converted $^{18}O_2$) during reaction of ethane and $^{18}O_2$ mixture at 573 K on $Mo_{0.61}V_{0.31}Nb_{0.08}{}^{16}O_x/Ti^{16}O_2$. C_2H_6: 533 kPa; $^{18}O_2$: 107 kPa; $H_2{}^{16}O$: 320 kPa.

Reactions of $C_2H_6/^{18}O_2/H_2{}^{16}O$ mixtures on $Mo_{0.61}V_{0.31}Nb_{0.08}{}^{16}O_x/Ti^{16}O_2$ were used to confirm the involvement of bulk lattice oxygen atoms in ethane oxidation. The involvement of bulk lattice oxygen led to ^{16}O isotopomers for all products at short contact times, and to a gradual increase in their ^{18}O content as bulk lattice ^{16}O atoms were replaced by ^{18}O atoms from the $^{18}O_2$ coreactants prevalent in the reactant mixture. $C_2H_6/^{18}O_2/H_2{}^{16}O$ reactions on $Mo_{0.61}V_{0.31}Nb_{0.08}{}^{16}O_x/Ti^{16}O_2$ led to products with identical isotopic content (including water), whereas $^{18}O_2$ remained essentially unmixed with the ^{16}O atoms present initially within the water added or the oxide lattice. The ($^{16}O/^{18}O$) ratio in all products was proportional to that in reactants (^{16}O atoms in added $H_2{}^{16}O/^{18}O$ atoms in $^{18}O_2$ reacted) at each contact time, indicating that isotopic scrambling between products and $H_2{}^{16}O$ is facile (Figure 5). Thus, conclusions about the sole involvement of lattice oxygen from these experiments are not definitive, because ^{16}O atoms in $H_2{}^{16}O$ are present in such a large excess relative to that in bulk lattice oxygen ($^{16}O_L$). The significant participation of bulk lattice oxygens is suggested, however, by the nonzero value of the ($^{16}O/^{18}O$) ratios as the (^{16}O in added $H_2{}^{16}O/^{18}O$ in converted $^{18}O_2$) ratio becomes zero at long contact times, which reflects an excess amount of ^{16}O in products, presumably arising from contributions by lattice oxygen atoms.

Reactions of $C_2H_6-{}^{18}O_2$ mixtures without added water were also examined to avoid the inaccuracies caused by the rapid exchange of lattice oxygen with H_2O on $Mo_{0.61}V_{0.31}Nb_{0.08}{}^{16}O_x/Ti^{16}O_2$ in the experiments described in the previous paragraph. These measurements were carried out at lower temperatures (473−523 vs 573 K) and with larger catalyst amounts that in other experiments reported here in an effort to detect product isotopomers well before significant depletion of lattice ^{16}O atoms by oxidation reactions. Figure 6 shows $^{16}O/^{18}O$ ratios in H_2O, CO, CO_2, and CH_3COOH products as a function of the amount of bulk ^{16}O removed from the lattice. These $^{16}O/^{18}O$ ratios in products were initially large (>6.0), indicating that they formed predominantly using lattice O atoms, initially present as ^{16}O, but decreased with contact time as bulk ^{16}O atoms were replaced by ^{18}O from $^{18}O_2$. $^{16}O^{18}O$ isotopomers were not detected, consistent with slow recombinative desorption of lattice O atoms. The involvement of bulk ^{16}O atoms and their appearance within initial reaction products reflect fast diffusion of oxygens between bulk and surface lattice positions. The total number of ^{16}O atoms in reaction products corresponds to a $Mo_{0.61}$-

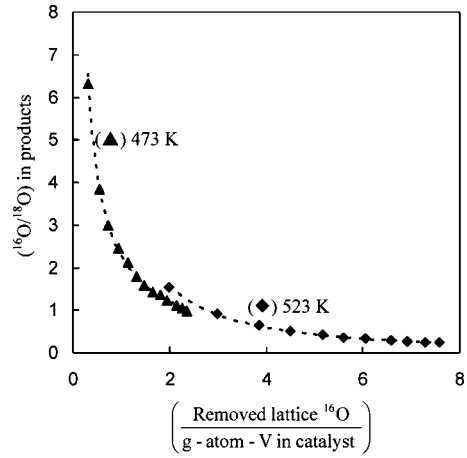

Figure 6. ($^{16}O/^{18}O$) ratio in the products (CH_3COOH, CO_2, CO, and H_2O) as a function of ^{16}O removed from catalyst lattice during ethane oxidation at 523 and 473 K on $Mo_{0.61}V_{0.31}Nb_{0.08}{}^{16}O_x/Ti^{16}O_2$ under anhydrous conditions. C_2H_6: 533 kPa; $^{18}O_2$: 107 kPa.

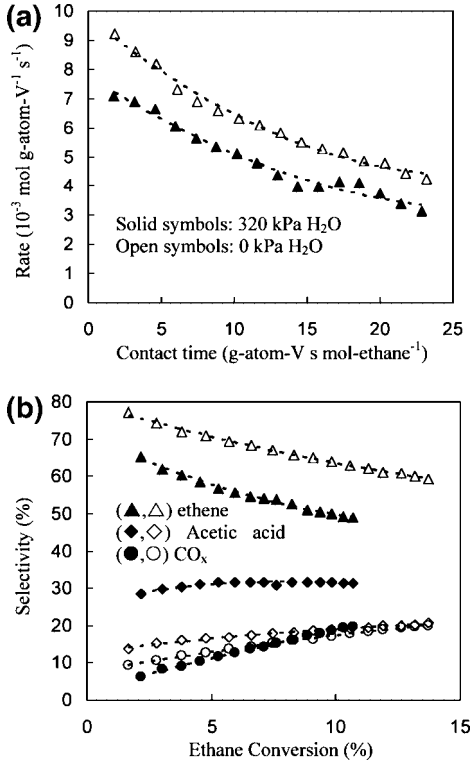

Figure 7. Ethane oxidation on $Mo_{0.61}V_{0.31}Nb_{0.08}O_x/TiO_2$ at 573 K in the presence of 320 kPa of H_2O and in the absence of H_2O. C_2H_6: 533 kPa; O_2: 107 kPa. (a) Ethane conversion rates versus contact time. (b) Selectivities of ethene, acetic acid, and CO_x as a function of ethane conversion.

$V_{0.31}Nb_{0.08}O_{2.8}$ stoichiometry, consistent with Mo_5O_{14} structures,[22–24] and with all oxygen atoms in the active oxides either exposed at surfaces or able to exchange with those exposed and able to participate in the redox cycles required for ethane oxidation.

3.3. Promotion and Inhibition of Ethane Oxidation Rates by Products. H_2O molecules formed during ethane oxidation or added to reactant mixtures increased acetic acid selectivities on Mo−V−Nb oxides.[1,6] The absence of water led to larger (ethene/acetic acid) ratios in products and to slightly higher CO_x selectivities (Figure 7). Primary rate constants (k_1, k_2, and k_4, Scheme 1) are shown in Table 1 for experiments in which either 0 or 320 kPa H_2O was initially present among C_2H_6/O_2 reactants.

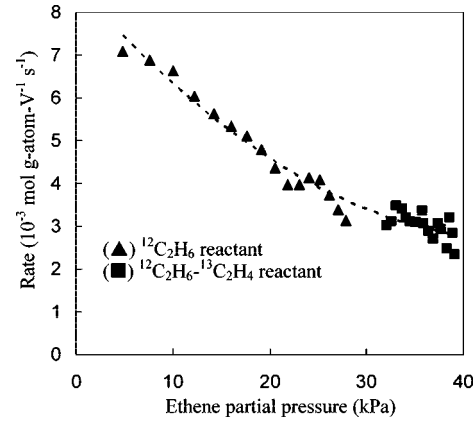

Figure 8. Dependence of ethane conversion rates on the partial pressures of ethene at 573 K on $Mo_{0.61}V_{0.31}Nb_{0.08}O_x/TiO_2$. $^{12}C_2H_6$: 533 kPa; $^{13}C_2H_4$: 32 kPa; O_2: 107 kPa; H_2O: 320 kPa.

H_2O decreased the rate constants for ethane oxidation to ethene (k_1; from 1.4×10^{-5} to 0.96×10^{-5} mol g-atom-V^{-1} s^{-1} kPa^{-1}) and CO_x (k_4; from 0.15×10^{-5} to 0.07×10^{-5} mol g-atom-V^{-1} s^{-1} kPa^{-1}), while increasing that for acetic acid synthesis (k_2; from 0.26×10^{-5} to 0.40×10^{-5} mol g-atom-V^{-1} s^{-1} kPa^{-1}). Thus, the promoting effect of water on acetic acid selectivity reflects a specific increase in the rate at which ethane converts to acetic acid via direct pathways. It seems plausible that water leads to higher coverages of *OH species (via step 9 in Scheme 2) and favors the desorption of acetate species as acetic acid (step 8 in Scheme 2), leading to its preferential formation during a single surface sojourn (initial acetic acid selectivity: 31% for 320 kPa H_2O and 14% for 0 kPa H_2O). The inhibition of ethane activation rates by water reflects, in turn, the titration of vacancies by water (through the reverse of step 9 in Scheme 2), which inhibits their reoxidation, as also shown during oxidative dehydrogenation of alkanes on MoO_x and VO_x catalysts.[18,25]

Ethane oxidation rates and selectivities on $Mo_{0.61}V_{0.31}Nb_{0.08}O_x/TiO_2$ did not change with time on stream in flow reactor experiments (573 K, 24 h). Yet, ethane oxidation rates decreased with contact time in gradientless batch reactor studies. These effects were stronger than expected from reactant depletion with the measured kinetic orders in C_2H_6 and O_2 (Figure 7; a 2-fold rate decrease at ∼10% ethane conversion). Thus, reaction products other than water, which is present in excess (320 kPa), must also inhibit reaction rates. These inhibition effects were probed by measuring rates of primary oxidation of $^{12}C_2H_6$ to ethene, acetic acid, and CO_x in the presence or absence of $^{13}C_2H_4$ or $^{13}CH_3{}^{13}COOH$ (32 kPa).

The presence of 32 kPa $^{13}CH_3{}^{13}COOH$ (equivalent to that prevalent at 20% conversion) decreased ethane oxidation rates only slightly (from 7.6×10^{-5} to 6.6×10^{-5} mol g-atom-V^{-1} s^{-1}) on $Mo_{0.61}V_{0.31}Nb_{0.08}O_x/TiO_2$, without any detectable changes in the acetic acid selectivity formed from ethane (31 vs 33%). These weak inhibition effects may reflect the capping of vacancies by acetic acid (via Step 8 in Scheme 2), but they cannot account for the marked changes in rate with contact time evident from the data in Figure 7.

The presence of 32 kPa $^{13}C_2H_4$, equivalent to that at ∼12% ethane conversion, led to a 2-fold decrease in ethane oxidation rates without detectable changes in selectivities (Figure 8). In the presence of $^{13}C_2H_4$, ethane oxidation rates did not decrease with increasing conversion, because ethene concentrations did not change significantly with time. These inhibition effects by

ethene may reflect rapid reactions of ethene with OH* to form higher surface coverages of ethoxide (step 3 in Scheme 2), which form acetaldehyde and acetic acid (steps 4−8 in Scheme 2); these steps are considerably faster than ethane activation steps and consume additional oxygen atoms. The resulting increase in the rate of depletion of O* appears to be responsible for the lower ethane oxidation rates, which may no longer occur on oxygen-saturated surfaces as ethene concentrations increase with increasing ethane conversion or when ethene is co-fed with ethane reactants.

4. Conclusions

Primary rate constants for ethane oxidation to ethene, acetic acid, and CO_x were measured by extrapolating their formation rates to zero contact time. Sequential reaction rate constants (k_{3eff} and k_5 and k_6 in Scheme 1) were determined from rates of formation of ^{13}C-labeled acetic acid and CO_x during oxidation of $^{13}C_2H_4/^{12}C_2H_6$ or $^{13}CH_3{}^{13}COOH/^{12}C_2H_6$ mixtures. The precipitation of active components ($Mo_{0.61}V_{0.31}Nb_{0.08}O_x$) in the presence of colloidal TiO_2 led to 10-fold increases in all rate constants (per active component), consistent with higher dispersion of active components similar in structure and surface reactivity to those present in bulk powders. PdO_x cocatalysts present as physical mixtures with $Mo_{0.61}V_{0.31}Nb_{0.08}O_x$ selectively increased the rate constant for ethene oxidation to acetic acid without a commensurate increase in ethene conversion to CO_x. Kinetic and isotopic studies showed that C−H bond activation in ethane by surfaces essentially saturated with lattice oxygens is the sole kinetically relevant step in ethane oxidation. These conclusions are consistent with the dependence of rates on O_2 and ethane pressures, with the normal kinetic isotope effects observed, and with the predominant initial presence of ^{16}O in all oxygenated products formed in reactions of $^{18}O_2/C_2H_6$ mixtures on $Mo_{0.61}V_{0.31}Nb_{0.08}{}^{16}O_x/Ti{}^{16}O_2$. Water increases acetic acid selectivities by promoting the desorption of acetate species as acetic acid. Ethene inhibits ethane oxidation rates via its competitive depletion of lattice oxygens in fast oxidation reactions, which decreases the rates of all primary and secondary reactions that require active oxygens provided by the $Mo_{0.61}V_{0.31}Nb_{0.08}O_x$ lattice.

Appendix

The selectivities and reaction rates of ethane oxidation reactions can be described for the reactions in Scheme 1, in which all reactions are assumed to be first-order dependence in the respective organic substrates and zero-order in O_2:

$$r_i = k_i \cdot P_x \tag{1a}$$

where r_i is the rate of reaction i, P_x is the partial pressure of organic reactant (x), and k_i is the first-order rate constant for step i in Scheme 1. Acetaldehyde is formed in trace amounts; thus, assuming that their concentrations are at steady state leads to an effective rate constant k_{3eff}:[4]

$$k_{3eff} = \frac{k_{31}}{1 + \frac{k_{33}}{k_{32}}} \cong k_{31} \tag{2a}$$

The rates of ethane consumption, ethene formation, and acetic acid formation with reaction residence time are given by:

$$\frac{1}{P^0_{C_2H_6}} \cdot \frac{dP_{C_2H_6}}{d\tau} = -r_1 - r_2 - r_4 = -(k_1 + k_2 + k_4) \cdot P_{C_2H_6} \tag{3a}$$

$$\frac{1}{P^0_{C_2H_6}} \cdot \frac{dP_{C_2H_6}}{d\tau} = -r_1 - r_3 - r_5 = k_1 \cdot P_{C_2H_6} - (k_{3eff} + k_5) \cdot P_{C_2H_6} \tag{4a}$$

$$\frac{1}{P^0_{C_2H_6}} \cdot \frac{dP_{CH_3COOH}}{d\tau} = r_2 + r_3 - r_6 = k_2 \cdot P_{C_2H_6} + k_{3eff} \cdot P_{C_2H_6} - k_6 \cdot P_{CH_3COOH} \tag{5a}$$

where $P^0_{C_2H_6}$ is the initial ethane partial pressure and τ (g-atom-V s mol-ethane^{-1}) is the contact time. These equations lead to reactant and product pressures given by:

$$P_{C_2H_6} = P^0_{C_2H_6} \cdot e^{-(k_1+k_2+k_4)\cdot P^0_{C_2H_6}\cdot\tau} \tag{6a}$$

$$P_{C_2H_4} = \frac{k_1 \cdot P^0_{C_2H_6}}{(k_{3eff} + k_5) - (k_1 + k_2 + k_4)} \cdot \left(e^{-(k_1+k_2+k_4)\cdot P^0_{C_2H_6}\cdot\tau} - e^{-(k_{3eff}+k_5)\cdot P^0_{C_2H_6}\cdot\tau}\right) \tag{7a}$$

$$P_{CH_3COOH} = \frac{(k_2 \cdot ((k_{3eff} + k_5) - (k_1 + k_2 + k_4)) + k_1 \cdot k_{3eff}) \cdot P^0_{C_2H_6}}{[(k_{3eff} + k_5) - (k_1 + k_2 + k_4)] \cdot (k_1 + k_2 + k_4 - k_6)} \cdot \left(e^{-k_6\cdot P^0_{C_2H_6}\cdot\tau} - e^{-(k_1+k_2+k_4)\cdot P^0_{C_2H_6}\cdot\tau}\right) - \frac{k_1 \cdot k_{3eff} \cdot P^0_{C_2H_6}}{[(k_{3eff} + k_5) - (k_1 + k_2 + k_4)] \cdot (k_{3eff} + k_5 - k_6)} \cdot \left(e^{-k_6\cdot P^0_{C_2H_6}\cdot\tau} - e^{-(k_3+k_5)\cdot P^0_{C_2H_6}\cdot\tau}\right) \tag{8a}$$

The selectivities of ethene and acetic acid changing with contact time are then:

$$S_{C_2H_4} = \frac{P_{C_2H_4}}{P^0_{C_2H_6} - P_{C_2H_6}} = \frac{\frac{k_1}{(k_{3eff} + k_5) - (k_1 + k_2 + k_4)} \cdot \left(e^{-(k_1+k_2+k_4)\cdot P^0_{C_2H_6}\cdot\tau} - e^{-(k_{3eff}+k_5)\cdot P^0_{C_2H_6}\cdot\tau}\right)}{1 - e^{-(k_1+k_2+k_4)\cdot P^0_{C_2H_6}\cdot\tau}} \tag{9a}$$

$$S_{CH_3COOH} = \frac{P_{CH_3COOH}}{P^0_{C_2H_6} - P_{C_2H_6}} = \left[\frac{(k_2 \cdot ((k_{3eff} + k_5) - (k_1 + k_2 + k_4)) + k_1 \cdot k_{3eff}}{[(k_{3eff} + k_5) - (k_1 + k_2 + k_4)] \cdot (k_1 + k_2 + k_4 - k_6)} \cdot (e^{-k_6 \cdot P^0_{C_2H_6} \cdot \tau} - e^{-(k_1+k_2+k_4) \cdot P^0_{C_2H_6} \cdot \tau}) - \frac{k_1 \cdot k_{3eff}}{[(k_{3eff} + k_5) - (k_1 + k_2 + k_4)] \cdot (k_{3eff} + k_5 - k_6)} \cdot (e^{-k_6 \cdot P^0_{C_2H_6} \cdot \tau} - e^{-(k_3+k_5) \cdot P^0_{C_2H_6} \cdot \tau})\right] \Big/ [1 - e^{-(k_1+k_2+k_4) \cdot P^0_{C_2H_6} \cdot \tau}] \quad (10a)$$

Acknowledgment. This manuscript is dedicated to the memory of Dr. Paul B. Plouffe, a friend and colleague. His words and his example taught us to convey substance and scholarship clearly and elegantly, but without pretence. We acknowledge the financial support of ExxonMobil Research and Engineering Co.

References and Notes

(1) Thorsteinson, E. M.; Wilson, T. P.; Young, F. G.; Kasai, P. H. *J. Catal.* **1978**, *52*, 116.
(2) Paulik, F. E.; Roth, J. F. *J. Chem. Soc., Chem. Commun.* **1968**, 1578.
(3) Li, X.; Iglesia, E. *Chem.−Eur. J.* **2007**, *13*, 9324.
(4) Li, X.; Iglesia, E. *Angew. Chem.* **2007**, *119*, 8803; *Angew. Chem., Int. Ed.* **2007**, *46*, 8649.
(5) Li, X.; Iglesia, E. *Appl. Catal., A* **2008**, *334*, 339.
(6) Linke, D.; Wolf, D.; Baerns, M.; Timpe, O.; Schlögl, R.; Zeyβ, S.; Dingerdissen, U. *J. Catal.* **2002**, *205*, 16.
(7) Al-Saeedi, J. N.; Guliants, V. V. *Appl. Catal., A* **2002**, *237*, 111.
(8) Al-Saeedi, J. N.; Guliants, V. V.; Vasudevan, V. K. *Catal. Commun.* **2003**, *4*, 537.
(9) Al-Saeedi, J. N.; Guliants, V. V.; Guerrero, O.; Bañares, M. A. *J. Catal.* **2003**, *215*, 108.
(10) Solsona, B.; López Nieto, J. M.; Oliver, J. M.; Gumbau, J. P. *Catal. Today* **2004**, *91−92*, 247.
(11) Botella, P.; López Nieto, J. M.; Solsona, B.; Mifsud, A.; Márquez, F. *J. Catal.* **2002**, *209*, 445.
(12) Karim, K.; Al-Hazmi, M.; Khan, A. U.S. Patent 6,060,421, 2000.
(13) Borchert, H.; Dingerdissen, U., DE Patent 19,745,902, 1997.
(14) Price, G. L.; Iglesia, E. *Ind. Eng. Chem. Res.* **1989**, *28*, 839.
(15) Ruth, K.; Burch, R.; Kieffer, R. *J. Catal.* **1998**, *175*, 27.
(16) Galownia, J. M.; Wight, A. P.; Blanca, A.; Labinger, J. A.; Davis, M. E. *J. Catal.* **2005**, *236*, 356.
(17) Oyama, S. T. *J. Catal.* **1991**, *128*, 210.
(18) Chen, K.; Khodakov, A.; Yang, J.; Bell, A. T.; Iglesia, E. *J. Catal.* **1999**, *186*, 325.
(19) Argyle, M. D.; Chen, K.; Bell, A. T.; Iglesia, E. *J. Phys. Chem. B* **2002**, *106*, 5421.
(20) Chen, K.; Iglesia, E.; Bell, A. T. *J. Phys. Chem. B* **2001**, *105*, 646.
(21) Chen, K.; Iglesia, E.; Bell, A. T. *J. Catal.* **2000**, *192*, 197.
(22) Merzouki, M.; Bordes, E.; Taouk, B.; Monceaux, L.; Courtine, P. *Stud. Surf. Sci. Catal.* **1992**, *72*, 81.
(23) Dieterle, M.; Mestl, G.; Jäger, J.; Uchida, Y.; Hibst, H.; Schlögl, R. *J. Mol. Catal. A: Chem.* **2001**, *174*, 169.
(24) Mestl, G.; Linsmeier, Ch.; Gottschall, R.; Dieterle, M.; Find, J.; Herein, D.; Jäger, J.; Uchida, Y.; Schlögl, R. *J. Mol. Catal. A: Chem.* **2000**, *162*, 463.
(25) Oyama, S. T.; Middlebrook, A. M.; Somorjai, G. A. *J. Phys. Chem.* **1990**, *94*, 5029.

JP801488Y